Letter

Strong coupling of lattice and orbital excitations in the quantum magnet $Ca_{10}Cr_7O_{28}$: Anomalous temperature dependence of Raman phonons

Srishti Pal,[1,*] Arnab Seth,[2,3] Anzar Ali,[4] Yogesh Singh,[4] D. V. S. Muthu,[1] Subhro Bhattacharjee,[2] and A. K. Sood[1]

[1]*Department of Physics, Indian Institute of Science, Bengaluru 560012, India*

[2]*International Centre for Theoretical Sciences, Tata Institute of Fundamental Research, Bengaluru 560089, India*

[3]*School of Physics, Georgia Institute of Technology, Atlanta, Georgia 30332, USA*

[4]*Indian Institute of Science Education and Research (IISER) Mohali, Knowledge City, Sector 81, Mohali 140306, India*

(Received 13 August 2023; revised 14 November 2023; accepted 17 November 2023; published 8 December 2023)

We report low-temperature Raman signatures of the Heisenberg quantum magnet $Ca_{10}Cr_7O_{28}$, showing clear anomalies in phonon mode frequencies and linewidths below ∼100 K. This crossover temperature lies in between the Jahn-Teller (JT) temperature scale (>room temperature) and the temperature scale associated with the spin exchange interactions (<12 K). Our experimental observation is well captured by a secondary JT transition associated with a cooperative reorientation of the orbitals giving rise to anomalies in the temperature dependence of Raman frequencies and linewidths. Such orbital reorganization, in turn, affects the spin-spin exchange interactions that decide the fate of the magnet at lower temperatures and hence provide important clues to understand the energetics of the possible lower-temperature quantum paramagnetic phase.

DOI: 10.1103/PhysRevB.108.L241103

Recent advances have invigorated vitality to the intricate interplay of different degrees of freedom giving rise to intervening coupling schemes in frustrated spin systems [1–3]. In particular, the role of these couplings in shaping the fate of geometrically frustrated spin-$\frac{1}{2}$ antiferromagnets—originally conceptualized [4] as suitable platforms for realizing quantum spin liquid (QSL) states [5–8]—have been thoroughly investigated both experimentally as well as on theoretical grounds on a large number of known *geometrically frustrated motifs* such as triangular [9–12], kagome [13–15], or pyrochlore [16,17]. One important factor bearing the potential to alter the spin exchange interactions in these frustrated magnets with complex structures is orbital interactions [18]. Some of the magnetic perovskites such as $KCuF_3$, $LaMnO_3$, and $BaVS_3$ had been studied previously for their coupling between the magnetic and orbital orderings responsible in minimizing the destabilizing two-electron two-orbital interactions [19–21].

In this regard, the quasi-two-dimensional Heisenberg quantum magnet $Ca_{10}Cr_7O_{28}$ [22–25] on bilayer kagome lattice presents a rather unique case disparate from the previously studied candidate geometrically frustrated QSLs. The compound with actual stoichiometry $Ca_{10}(Cr^{V}O_4)_6(Cr^{VI}O_4)$ [26] contains magnetically isolated distorted kagome bilayers of spin-$\frac{1}{2}$ Cr^{5+} ions with both ferromagnetic (FM) and antiferromagnetic (AFM) isotropic Heisenberg exchange couplings [22–24]. The magnetic Hamiltonian constructed as a combination of experimental phenomenology and first principle calculations that accounts for the inequivalent FM (significantly stronger) and AFM isotropic Heisenberg couplings ($\Sigma J \lesssim 1$ meV) [24] results in a mean-field Curie-Weiss temperature of $\theta_{CW} \approx 4$ K that is corroborated by experiments which show a broad cusp like feature around $T \approx 3.1$ K in the magnetic specific heat [22,24,25,27–29]. However, the system shows no sign of long-range magnetic order or any spin-glass freezing down to 19 mK with a fluctuating spin liquid ground state as confirmed from bulk susceptibility, heat capacity, μSR, or neutron scattering measurements [22–24,28,30] as well as from theoretical studies [28,31,32]. Due to the complex structure of this compound, more careful observation needs to be performed to disentangle the contribution of spin and orbital moments to the underlying magnetic Hamiltonian, and also possibly the role of lattice degrees of freedom.

In this Letter, we report our Raman scattering results on polycrystalline samples of $Ca_{10}Cr_7O_{28}$ [see Supplemental Material (SM) [33] for details on sample synthesis] down to ∼4 K, revealing that strong anomalies in the temperature dependence of phonon frequencies and linewidths, at the crossover temperature $T_C \sim 100$ K, much above the temperature scale (∼10 K) associated with the spin exchange interactions, hence cannot arise from nontrivial spin-phonon coupling, since the spins, for all practical purposes, are deep inside the thermal paramagnet, i.e., effectively at infinite temperature ($T/\Theta_{CW} \gg 1$). Therefore, these Raman anomalies are very much different from the temperature-induced magnetic ordering transitions [34,35] which are strictly absent in the $Ca_{10}Cr_7O_{28}$ system [23]. This raises the central question about the origin of this energy scale and the associated Raman-active phonon renormalization, and here we show that this is naturally attributed to phonon-orbital coupling via a cascade of Jahn-Teller effects, both single ion and cooperative.

To begin the search for the physics of the 100 K energy scale, it is worth noting that the system contains Jahn-Teller (JT)-active [36] Cr^{5+} ion sites offering moderately distorted $Cr^{V}O_4$ tetrahedra even at room temperature and down to 2 K without any further structural distortion throughout the temperature range as reported in earlier studies [23,37].

*srishtipal@iisc.ac.in

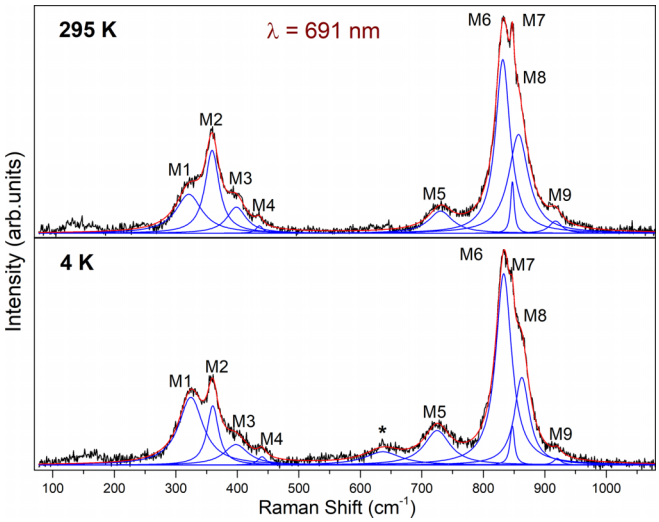

FIG. 1. The two panels show phonon fits to the Raman spectra at 295 and 4 K. Experimental data are indicated by black curves. Blue and red curves are individual phonon modes and the cumulative fits, respectively. The asterisk (*) represents the new mode appearing at 4 K.

Therefore, the 100 K phonon anomalies cannot be attributed to the thermal order-disorder crossover from a static to dynamic JT effect which is associated with symmetry-raising-type structural transitions [38–40]. Hence, we turn our focus on the cooperative JT effect driven by the interaction between localized orbitals and the crystal lattice [41,42]. Such Raman fingerprints in terms of the splitting of Raman bands for the cooperative JT effect have been reported previously in rare-earth compounds such as $DyVO_4$, $DyAsO_4$, and $TbVO_4$ [43], where the transitions are associated with only small lattice strains and the splitting of the ground electronic states of the active ions. Here, we present our detailed experimental observation of these intermediate-temperature phenomena and support it with theoretical calculations under the framework of the cooperative JT effect to derive the phonon renormalization induced by an orbital reordering phenomenon [44–46] emerging from the significant coupling between the vibrational and orbital degrees of freedom. Such reordering has direct implications on the spin physics of this frustrated magnet at even lower temperature via a drastic renormalization of the spin-spin exchanges.

Raman spectra of $Ca_{10}Cr_7O_{28}$ at 4 and 295 K are shown in Fig. 1 along with the phonon fits. A factor group analysis of trigonal ($R3c$) $Ca_{10}Cr_7O_{28}$ yields 139 Raman-active phonon modes ($\Gamma_{\text{Raman}} = 46A_{1g} + 93E_g$) among which nine modes could be detected at 295 K in the frequency range 75–1000 cm^{-1}. From earlier reports on compounds containing $Cr^{V}O_4$ tetrahedra [47,48], we assign the low- (M1–M4) and high- (M5–M9) frequency vibrational bands of $Ca_{10}Cr_7O_{28}$ as bending and stretching modes of the $Cr^{V}O_4$ tetrahedra, respectively. More details on mode assignment using polarized Raman scattering [49] are given in the SM [33].

The phonon modes are fitted with a symmetric Lorentzian profile function for the entire range of temperature. The phonon spectrum remains unchanged with decreasing temperature except only at the lowest temperature of 4 K where one new weak mode at ∼640 cm^{-1} [indicated by (*) in the lower panel of Fig. 1] could be detected. The appearance of a new phonon mode in the Raman spectrum can indicate a possible symmetry-lowering structural transition, but for the present $Ca_{10}Cr_7O_{28}$ system, we can discard this possibility owing to the neutron time-of-flight (TOF) powder diffraction studies reported by Balz *et al.* [23] which confirmed the absence of any structural phase transition or lattice distortion down to 2 K. This temperature scale rather lines up with the anomalous cusplike feature observed in earlier heat-capacity studies [22,24,25,27–29] where it has been associated with the presence of coherent quantum fluctuations and the onset of short-range spin correlations during the crossover from a high-temperature paramagnetic to a low-temperature spin liquid regime [22]. Later in their semiclassical model, Biswas *et al.* [31] also pointed out that the specific heat anomaly can be explained in terms of the average of two crossover temperatures associated with the unbinding of the effective $S = \frac{3}{2}$ moments into three independent $S = \frac{1}{2}$ moments (since there exist two different ferromagnetic couplings in the two kagome layers of each bilayer).

The temperature evolution of frequencies and full width at half maxima (FWHM) for selected phonon modes is shown in Figs. 2(a) and 2(b). The solid orange curves are fits from 100 to 295 K to the simple cubic anharmonic model [50] (see SM [33] for fitting details). The dashed ones are their extensions to lower-temperature ranges. It is worth noting that except for M8, frequencies and FWHM of all other modes exhibit anomalous behavior with temperature. While frequencies of M1, M2, and FWHM of M1, M2, M5, and M6 show clear deviations from the expected cubic anharmonicity below ∼100 K, frequencies of M5 and M6 modes are anomalous throughout the entire temperature range and hence could not be fitted with the cubic anharmonic model. While M5 frequency shows a discontinuity around 100 K with a change in the slope, M6 frequency experiences a slope change around 100 K with a striking similarity in its temperature profile with that of its linewidth. Apart from the strong anomalies in frequencies and linewidths, the phonon modes show subtle anomalous behavior in the temperature dependence of their integrated susceptibilities as shown in SM [33] (see also Ref. [51] therein).

As remarked above, the crossover temperature of ∼100 K associated with the strong phonon anomalies in the $Ca_{10}Cr_7O_{28}$ system is too high to be linked with the spin exchange interactions with a temperature scale of ∼10 K and below. Also, as discussed earlier, the neutron TOF studies [23] confirmed the absence of any structural changes down to 2 K. However, an interesting observation regarding the $Ca_{10}Cr_7O_{28}$ crystal system is that its $Cr^{V}O_4$ tetrahedra are distorted at room temperature, bearing four different Cr-O bond lengths (see SM [33]). This can be understood by noting that the Cr^{5+} in a tetrahedral crystal field has one electron in the e_g orbitals and hence is a Jahn-Teller (JT)-active ion [36]. The degeneracy of the atomic orbitals is therefore susceptible to JT splitting associated with the distortion of the tetrahedra (see Fig. S2 in SM [33]).

The above experimental phenomenology poses the following question: Is the ∼100 K scale seen by the phonons related to the JT rearrangement of the orbitals due to various

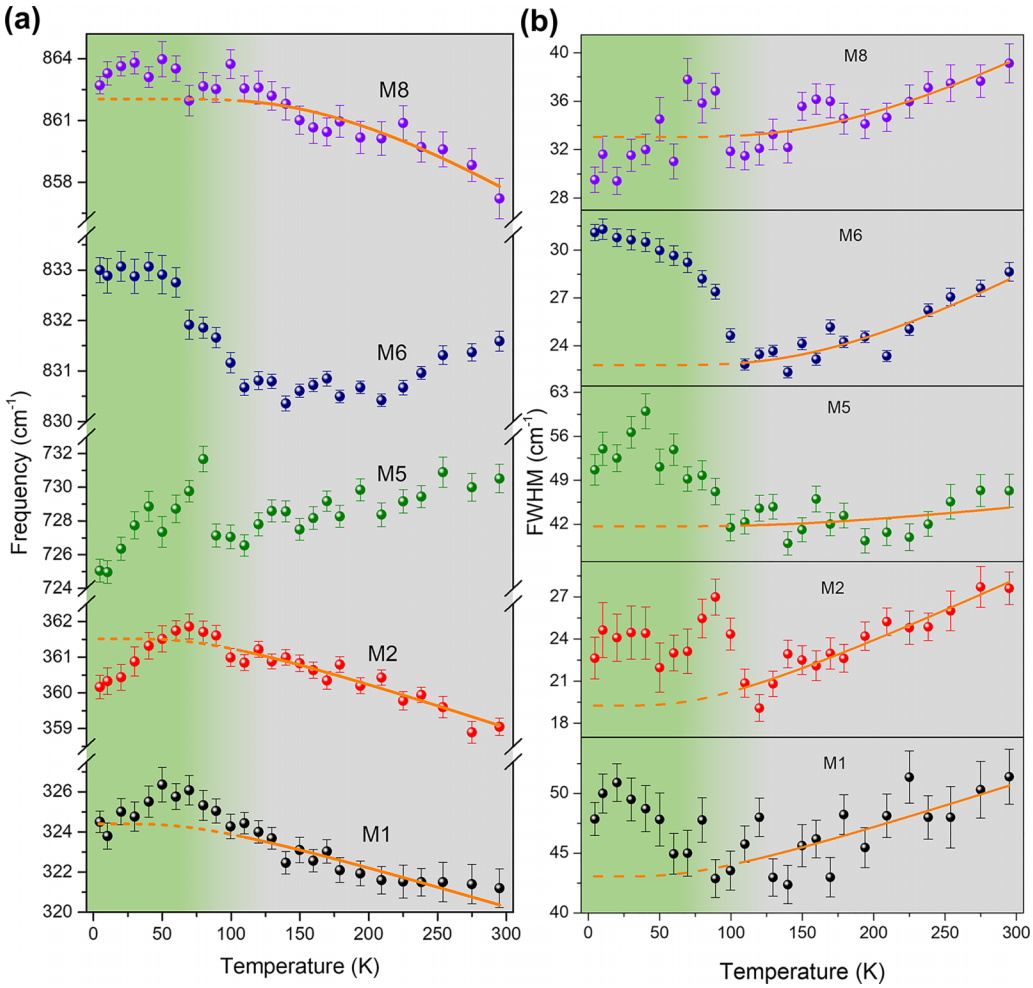

FIG. 2. Temperature dependence of (a) frequencies and (b) linewidths of selected phonon modes. The orange curves are fits to the cubic anharmonic model with $\omega_{\rm anh}^{(p)} = \omega_0 + A[1 + 2n(\frac{\omega_0}{2})]$ and $\Pi_{\rm anh}^{(p)} = \Gamma_0 + B[1 + 2n(\frac{\omega_0}{2})]$. Details of the parameters are given in the SM [33].

orbital-lattice couplings? Indeed, the different vibrational modes allow for such *secondary cooperative* JT distortions. Below, we explore the possibility of such physics to explain the phenomenology of $Ca_{10}Cr_7O_{28}$ via minimal symmetry-allowed Hamiltonians.

A minimal model that captures the above JT distortion includes the spin-$\frac{1}{2}$, S_i^α, and the two e_g orbitals $[(|d_{3z^2-r^2}\rangle, |d_{x^2-y^2}\rangle) \equiv (|+\rangle, |-\rangle)]$ τ_i^α on the Cr^{5+} sites as well as the Raman-active phonons ϵ_i^p (p denotes the normal modes) with appropriate symmetries. The associated spin-orbital-phonon Hamiltonian is given by $H = H_{S,\tau,\epsilon} + H_\epsilon$, where H_ϵ is the harmonic phonon Hamiltonian and

$$H_{S,\tau,\epsilon} = \sum_{\langle ij \rangle} \left[K_{ij}^{\alpha\beta} + J_{ij}^{\alpha\beta} \mathbf{S}_i \cdot \mathbf{S}_j\right] \tau_i^\alpha \tau_j^\beta + \sum_i \Gamma^{p,\beta} \epsilon_i^p \tau_i^\beta, \quad (1)$$

with $J_{ij}^{\alpha\beta}$ and $K_{ij}^{\alpha\beta}$ denoting the bare spin-spin and orbital-orbital exchange interactions, respectively, between two neighboring Cr^{5+} ions; $\Gamma^{p,\beta}$ is the coupling of the orbitals with the phonon modes. Note that, due to the absence of atomic spin-orbit coupling (expected to be small for $3d$ transition metals), the spin-spin interactions are rotationally symmetric while the dependence on the orbital labels is constrained by lattice symmetries. The second term denotes the symmetry-allowed linear coupling between the orbitals and the phonon modes that is present in a JT-active ion and is responsible for the distortion via $\epsilon^p = -\frac{\Gamma^{p,\beta}}{C_p}\tau^\beta$ (C_p is the spring constant of the phonon) along the direction determined by the largest JT coupling $\Gamma^{p,\beta}$ for the softest elastic mode. This in turn decides the specific splitting of the orbitals, i.e., $\langle \tau^\alpha \rangle \neq 0$.

Below the temperature scale of this *primary JT* splitting, the other JT coupling constants, as well as the orbital-coupling scale, can induce further *secondary JT* transitions which can be rendered cooperative due to $K_{ij}^{\alpha\beta}$. These successive JT transitions therefore lead to a rearrangement of the orbital ordering which, as explained below, we attribute to the experimentally observed Raman anomalies around $T \sim 100$ K.

Orbital fluctuations at intermediate temperatures. Consider the intermediate-temperature range where the Raman anomalies are observed, $\Theta_{\rm CW}(\sim 10\ {\rm K}) \ll T < T_H(>300\ {\rm K})$, where $\Theta_{\rm CW} \sim 10$ K and T_H are respectively the Curie-Weiss and the primary JT transition temperatures. In this temperature range, the spins form a thermal paramagnet, i.e., $\langle \mathbf{S}_i \rangle = 0$, and are completely incoherent. Therefore, their only effect is to renormalize the couplings $K_{ij}^{\alpha\beta}$ in Eq. (1) via short-ranged spin-spin correlations. However, the orbital ordering has set in due to the

primary JT effect. Let us assume that this ordering is along τ^z (we do not know the actual direction of distortion from the powder samples). Therefore, the effective Hamiltonian in the intermediate-temperature range is given by

$$\tilde{H} = \sum_{\langle ij \rangle} \mathcal{K}_{ij}^{\alpha\beta} \tau_i^\alpha \tau_j^\beta + \Delta_1 \sum_i \tau_i^z + \sum_i \Gamma^{p,\beta} \epsilon_i^p \tau_i^\beta + \tilde{H}_\epsilon, \quad (2)$$

where $\mathcal{K}_{ij}^{\alpha\beta} = K_{ij}^{\alpha\beta} + J_{ij}^{\alpha\beta} \langle \mathbf{S}_i \cdot \mathbf{S}_j \rangle$ is the effective exchange for the orbitals; Δ_1 characterizes the splitting of the orbitals due to the primary JT effect. In principle, there will also be a symmetry-allowed term of the form $\Delta_2 \sum_i \tau_i^x$ coming from the lattice distortion at the primary JT transition, but the effect of such terms is straightforward—they smear out the sharp features of phase transitions arising from Eq. (2) which makes way for a smooth crossover as seen in experiments [35,38,40].

In Eq. (2), the sum p now runs over the other phonon modes that can potentially lead to secondary cooperative JT mediated reordering via $\mathcal{K}_{ij}^{\alpha\beta}$, and $\tilde{H}_\epsilon$ is the harmonic phonon Hamiltonian for the phonons in the distorted state below the primary JT transition. Assuming a single secondary mode favoring an ordering along τ^x, the mean-field phase diagram [52] is easy to work out and is given in the SM [33] (see Fig. S3). In the mean-field approximation, the orbital reordering sets in below a temperature $T_c = (\mu^{xx} - \tilde{\mathcal{K}}^{xx}) \frac{\delta}{\tanh^{-1}(\delta)}$, where $\delta = \Delta_1/(\mu^{xx} - \tilde{\mathcal{K}}^{xx})$, $\tilde{\mathcal{K}}^{xx} = \mathcal{K}^{xx} D$ (D = coordination number), and $\mu^{xx} = \frac{\Gamma^{p,x}\Gamma^{p,x}}{C_p}$ are effective coupling constants [or below the dimensionless temperature $T_c/(\mu^{xx} - \tilde{\mathcal{K}}^{xx})$]. We associate T_c with ∼100 K with the experimentally observed onset scale of the phonon anomalies.

Phonon anomaly due to secondary JT transition. In the intermediate-temperature regime, the phonon anomalies observed in our vibrational Raman scattering experiments can be analyzed using the phonon-orbital coupling Hamiltonian which is given in detail in the SM [see Eq. (S5)]. For this, we note that in addition to $\Gamma^{p,\alpha}$, the orbital-phonon coupling has another source, i.e., the coupling constant $\mathcal{K}_{ij}^{\alpha\beta}$, which is dependent on the dynamic distortions of the tetrahedra and hence we have, similar to the usual magnetoelastic coupling,

$$\mathcal{K}_{ij}^{\alpha\beta} = \bar{\mathcal{K}}_{ij}^{\alpha\beta} + A_{ij}^{\alpha\beta;p}\left(\epsilon_i^p + \epsilon_j^p\right) + B_{ij}^{\alpha\beta;pq} \epsilon_i^p \epsilon_j^q, \quad (3)$$

where $A_{ij}^{\alpha\beta;p}$ and $B_{ij}^{\alpha\beta;pq}$ are coupling constants whose different components are constrained by the residual symmetries. Using this in the orbital Hamiltonian H_{orb}, we obtain the orbital-phonon coupling that is central to the vibrational Raman scattering (see SM [33]). The phonon renormalization can then be computed perturbatively due to these interactions.

The renormalization of phonon frequency and linewidth are respectively given by

$$\Delta\omega^{(p)} = \omega^{(p)} - \omega_0 = \Delta\omega_{\text{anh}}^{(p)} + \Delta\omega_{\text{orb}}^{(p)}, \quad (4)$$

$$\Pi^{(p)} = \left|\Pi_{\text{anh}}^{(p)} + \Pi_{\text{orb}}^{(p)}\right|, \quad (5)$$

where the subscripts "anh" and "orb" represent the contributions due to the anharmonic effects and orbital reordering, respectively. While the anharmonic contributions to the phonon parameters are usually determined from the fitting of the experimental data at high temperatures (see SM [33]), the orbital contribution can be computed within the Einstein (independent bond) approximation. The leading-order renormalization of the frequency is given by

$$\Delta\omega_{\text{orb}}^{(p)} \propto B_{ij}^{\beta\gamma;pp} \langle \tau_i^\beta \tau_j^\gamma \rangle, \quad (6)$$

where $\langle \cdots \rangle$ denotes the averaging over a Gibbs ensemble at temperature $1/\beta$. The phonon frequency renormalization due to orbital reordering, therefore, is determined by the equal-time orbital correlators on nearest neighbors. Within our minimal model, approximating $\langle \tau_i^x \tau_j^x \rangle \approx \langle \tau^x \rangle^2$, $\langle \tau_i^z \tau_j^z \rangle \approx \langle \tau^z \rangle^2$, and $\langle \tau_i^x \tau_j^z \rangle \approx \langle \tau^x \rangle \langle \tau^z \rangle$ below T_c, we obtain results that are plotted in Fig. 3 (top panel) as a function of temperature for various representative choices of the coupling constants. In particular, as is clear from these plots, the softening or hardening of the phonon is determined by the sign of the coupling $B_{ij}^{\beta\gamma;pp}$. We see both these behaviors for different phonons that are consistent with the experimental observation [see Fig. 2(a)]. An estimate of these coupling constants, however, requires a more microscopic calculation which is beyond the purview of the present symmetry-based arguments.

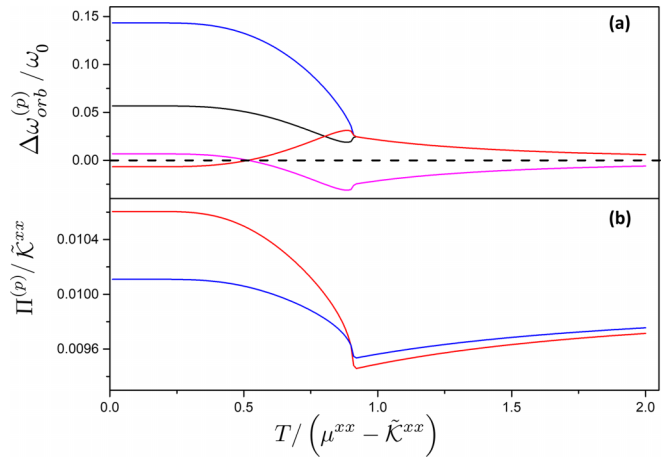

FIG. 3. (a) Frequency shift due to the orbital reordering. Blue, black, red, and magenta curves are obtained by choosing $(B^{xx;pp}, B^{zz;pp}, B^{xz;pp})/\omega_0$ to be (0.1,0.1,0.1), (0.1, 0.1, −0.1), (−0.1, 0.1, −0.1), and (0.1, −0.1, 0.1), respectively. (b) Linewidth renormalization of the phonon. For blue and red curves, we choose $\Gamma_0 = 0.01\tilde{\mathcal{K}}^{xx}$, $\mathcal{M}_{xx} = \mathcal{M}_{xz} = -0.7\tilde{\mathcal{K}}^{xx}$ and $\Gamma_0 = 0.01\tilde{\mathcal{K}}^{xx}$, $\mathcal{M}_{xx} = -0.6\tilde{\mathcal{K}}^{xx}$, $\mathcal{M}_{xz} = -0.4\tilde{\mathcal{K}}^{xx}$, respectively, and set all other parameters to zero. For both panels, $\delta = 0.5$. In the x axis, the temperature is scaled with respect to $(\mu^{xx} - \tilde{\mathcal{K}}^{xx})$.

Turning to the linewidths, we calculate them via well-known methods of diagrammatic perturbation theory from which the linewidth is given by the imaginary part of the phonon self-energy arising due to its scattering with τ_i^α's and determined by, to the leading order, the dynamic orbital correlation functions $\mathcal{C}_{\mu\nu}(\mathbf{r}, \tau) = \langle \hat{T}(\tau_{\mathbf{r}}^\mu(\tau)\tau_{\mathbf{0}}^\nu(0)) \rangle - \langle \tau_{\mathbf{r}}^\mu(\tau) \rangle \langle \tau_{\mathbf{0}}^\nu(0) \rangle$.

The resultant leading-order Raman linewidths are given by [53]

$$\Pi_{\text{orb}}^{(p)}(\omega) \sim \sum_{\mu,\nu=x,z} \mathcal{M}_{\mu\nu} \, \text{Im}[\tilde{\mathcal{C}}_{\mu\nu}(\mathbf{k} = 0, \omega + i0^+)], \quad (7)$$

where $\tilde{\mathcal{C}}_{\mu\nu}(\mathbf{k}, \omega + i0^+)$ is the Fourier transform of $\mathcal{C}_{\mu\nu}(\mathbf{r}, \tau)$ and $M_{\mu\nu}$ is the form factor whose form can be found in the

SM [33] [see Eq. (S8)]. For simplicity, in Fig. 3 (bottom panel) we plot the temperature dependence of the linewidth assuming these coefficients to be temperature independent, and therefore this is now completely controlled by the two-point dynamic correlators of the orbitals. We note that such behavior is in direct conformity with the experimental observation [see Fig. 2(b)].

In conclusion, we have explored temperature-induced Raman anomalies in polycrystalline samples of the Heisenberg quantum magnet $Ca_{10}Cr_7O_{28}$. The phonon mode frequencies, linewidths, and integrated intensities reveal clear anomalies across ∼100 K, a temperature scale much higher than the one associated with the spin exchange interactions of the system (<10 K). Considering the fact that the system is Jahn-Teller distorted above room temperature, we develop our theoretical understanding to realize the Raman anomalies to originate from an orbital reordering phenomenon, renormalizing the phonon self-energy via a cooperative Jahn-Teller effect. As we have used polycrystalline sample in our studies, we could not do an extensive assignment of different phonon modes to different vibrations (symmetries). In the future, polarization-dependent Raman studies on single crystals can help to understand the origin of the different natures of anomalies for different phonon modes. Also, resonant inelastic x-ray scattering measurements can be performed on the system as a function of temperature to capture the orbital ordering. In passing, we note that, once the orbitals are ordered at low temperature ($T < 100$ K), the effective spin Hamiltonian is obtained from Eq. (1) as $H_{\rm spin} = \sum_{ij} \mathcal{J}_{ij} \mathbf{S}_i \cdot \mathbf{S}_j + \cdots$, where $\mathcal{J}_{ij} = \sum_{\alpha\beta} J_{ij}^{\alpha\beta} \langle \tau_i^\alpha \rangle \langle \tau_j^\beta \rangle$ are the effective low-temperature spin-spin exchanges and $\cdots$ refers to other constant terms. This should result in a variation of the Curie-Weiss temperature and can account for the low effective spin-spin exchanges observed in $Ca_{10}Cr_7O_{28}$, which in turn dictates the fate of the spin state at lower temperatures. Thus, the secondary JT physics plays an important role in ultimately deciding the possible QSL state in the material.

Acknowledgement. A.K.S. thanks DST for financial support under a National Science Chair Professorship. A.S. and S.B. acknowledge funding from a Max Planck Partner Group grant at ICTS, Swarna Yayanti Fellowship Grant of SERB-DST (India) Grant No. SB/SJF/2021-22/12, and the Department of Atomic Energy, Government of India, under Project No. RTI4001.

[1] A. P. Ramirez, Strongly geometrically frustrated magnets, Annu. Rev. Mater. Sci. **24**, 453 (1994).
[2] L. Balents, Spin liquids in frustrated magnets, Nature (London) **464**, 199 (2010).
[3] C. Liu, R. Yu, and X. Wang, Semiclassical ground-state phase diagram and multi-Q phase of a spin-orbit-coupled model on triangular lattice, Phys. Rev. B **94**, 174424 (2016).
[4] P. W. Anderson, Resonating valence bonds: A new kind of insulator? Mater. Res. Bull. **8**, 153 (1973).
[5] L. Savary and L. Balents, Quantum spin liquids: A review, Rep. Prog. Phys. **80**, 016502 (2017).
[6] P. A. Lee, An end to the drought of quantum spin liquids, Science **321**, 1306 (2008).
[7] Y. Zhou, K. Kanoda, and T.-K. Ng, Quantum spin liquid states, Rev. Mod. Phys. **89**, 025003 (2017).
[8] J. Knolle and R. Moessner, A field guide to spin liquids, Annu. Rev. Condens. Matter Phys. **10**, 451 (2019).
[9] Y. Shimizu, K. Miyagawa, K. Kanoda, M. Maesato, and G. Saito, Spin liquid state in an organic Mott insulator with a triangular lattice, Phys. Rev. Lett. **91**, 107001 (2003).
[10] S. Yamashita, N. Nakata, Y. Kasahara, T. Sasaki, N. Yoneyama, N. Kobayashi, S. Fujimoto, T. Shibauchi, and Y. Matsuda, Thermal-transport measurements in a quantum spin-liquid state of the frustrated triangular magnet κ-(BEDT-TTF)$_2$Cu$_2$(CN)$_3$, Nat. Phys. **5**, 44 (2009).
[11] T. Itou, A. Oyamada, S. Maegawa, M. Tamura, and R. Kato, Quantum spin liquid in the spin-1/2 triangular antiferromagnet EtMe$_3$Sb[Pd(dmit)$_2$]$_2$, Phys. Rev. B **77**, 104413 (2008).
[12] Y. S. Li, H. Liao, Z. Zhang, S. Li, F. Jin, L. Ling, L. Zhang, Y. Zou, L. Pi, Z. Yang, J. Wang, Z. Wu, and Q. Zhang, Gapless quantum spin liquid ground state in the two-dimensional spin-1/2 triangular antiferromagnet YbMgGaO$_4$, Sci. Rep. **5**, 104413 (2015).
[13] J. S. Helton, K. Matan, M. P. Shores, E. A. Nytko, B. M. Bartlett, Y. Yoshida, Y. Takano, A. Suslov, Y. Qiu, J. H. Chung, D. G. Nocera, and Y. S. Lee, Spin dynamics of the spin-1/2 kagome lattice antiferromagnet ZnCu$_3$(OH)$_6$Cl$_2$, Phys. Rev. Lett. **98**, 107204 (2007).
[14] B. Fåk, E. Kermarrec, L. Messio, B. Bernu, C. Lhuillier, F. Bert, P. Mendels, B. Koteswararao, F. Bouquet, J. Ollivier, A. D. Hillier, A. Amato, R. H. Colman, and A. S. Wills, Kapellasite: A kagome quantum spin liquid with competing interactions, Phys. Rev. Lett. **109**, 037208 (2012).
[15] M. Fu, T. Imai, T.-H. Han, and Y. S. Lee, Evidence for a gapped spin-liquid ground state in a kagome Heisenberg antiferromagnet, Science **350**, 655 (2015).
[16] M. J. P. Gingras and P. A. McClarty, Quantum spin ice: A search for gapless quantum spin liquids in pyrochlore magnets, Rep. Prog. Phys. **77**, 056501 (2014).
[17] A. Scheie, J. Kindervater, S. Zhang, H. J. Changlani, G. Salac, G. Ehlers, A. Heinemannh, G. S. Tucker, S. M. Koohpayeh, and C. Broholm, Multiphase magnetism in Yb$_2$Ti$_2$O$_7$, Proc. Natl. Acad. Sci. USA **117**, 27245 (2020).
[18] H.-J. Koo and M.-H. Whangbo, Spin dimer analysis of the spin Eexchange interactions of the vanadium oxides AV_4O_9 (A = Ca, Sr, Cs$_2$, NH$_2$(CH$_2$)$_4$NH$_2$), J. Solid State Chem. **153**, 263 (2000).
[19] A. M. Oleś, M. Cuoco, and N. B. Perkins, Magnetic and orbital ordering in cuprates and manganites, AIP Conf. Proc. **527**, 226 (2000).
[20] M.-H. Whangbo and H.-J. Koo, Orbital interaction analysis of cooperative Jahn-Teller distortion, orbital ordering, spin ordering, and spin exchange interactions in magnetic solids, Solid State Sci. **4**, 335 (2002).
[21] M.-H. Whangbo, H.-J. Koo, D. Dai, and A. Villesuzanne, Analysis of the electron localization, the anisotropy of

electrical conductivity, the orbital ordering, and spin-exchange interactions in $BaVS_3$ on the basis of first principles and semi-empirical electronic structure calculations, J. Solid State Chem. **165**, 345 (2002).

[22] C. Balz, B. Lake, J. Reuther, H. Luetkens, R. Schönemann, T. Herrmannsdörfer, Y. Singh, A. T. M. N. Islam, E. M. Wheeler, J. A. Rodriguez-Rivera, T. Guidi, G. G. Simeoni, C. Baines, and H. Ryll, Physical realization of a quantum spin liquid based on a complex frustration mechanism, Nat. Phys. **12**, 942 (2016).

[23] C. Balz, B. Lake, M. Reehuis, A. T. M. N. Islam, O. Prokhnenko, Y. Singh, P. Pattison, and S. Tóth, Crystal growth, structure and magnetic properties of $Ca_{10}Cr_7O_{28}$, J. Phys.: Condens. Matter **29**, 225802 (2017).

[24] C. Balz, B. Lake, A. T. M. Nazmul Islam, Y. Singh, J. A. Rodriguez-Rivera, T. Guidi, E. M. Wheeler, G. G. Simeoni, and H. Ryll, Magnetic Hamiltonian and phase diagram of the quantum spin liquid $Ca_{10}Cr_7O_{28}$, Phys. Rev. B **95**, 174414 (2017).

[25] D. R. Alshalawi, J. M. Alonso, A. R. Landa-Cánovas, and P. de la Presa, Coexistence of two spin frustration pathways in the quantum spin liquid $Ca_{10}Cr_7O_{28}$, Inorg. Chem. **61**, 16228 (2022).

[26] I. Arčon, B. Mirtič, and A. Kodre, Determination of valence states of chromium in calcium chromates by using x-ray absorption near-edge structure (XANES) spectroscopy, J. Am. Ceram. Soc. **81**, 222 (1998).

[27] A. Balodhi and Y. Singh, Synthesis and pressure and field-dependent magnetic properties of the kagome-bilayer spin liquid $Ca_{10}Cr_7O_{28}$, Phys. Rev. Mater. **1**, 024407 (2017).

[28] J. Sonnenschein, C. Balz, U. Tutsch, M. Lang, H. Ryll, J. A. Rodriguez-Rivera, A. T. M. Nazmul Islam, B. Lake, and J. Reuther, Signatures for spinons in the quantum spin liquid candidate $Ca_{10}Cr_7O_{28}$, Phys. Rev. B **100**, 174428 (2019).

[29] A. Balodhi, A. Ali, and Y. Singh, Robustness of the spin liquid state with respect to magnetic dilution in the bilayer kagome material $Ca_{10}Cr_7O_{28}$, Phys. Rev. B **101**, 184416 (2020).

[30] J. M. Ni, Q. Y. Liu, Y. J. Yu, E. J. Cheng, Y. Y. Huang, Z. Y. Liu, X. J. Wang, Y. Sui, and S. Y. Li, Ultralow-temperature heat transport in the quantum spin liquid candidate $Ca_{10}Cr_7O_{28}$ with a bilayer kagome lattice, Phys. Rev. B **97**, 104413 (2018).

[31] S. Biswas and K. Damle, Magnetic Hamiltonian and phase diagram of the quantum spin liquid $Ca_{10}Cr_7O_{28}$, Phys. Rev. B **97**, 115102 (2018).

[32] R. Pohle, H. Yan, and N. Shannon, Theory of $Ca_{10}Cr_7O_{28}$ as a bilayer breathing-kagome magnet: Classical thermodynamics and semiclassical dynamics, Phys. Rev. B **104**, 024426 (2021).

[33] See Supplemental Material at http://link.aps.org/supplemental/10.1103/PhysRevB.108.L241103 for details on sample synthesis, methodology, fitting details, polarized Raman spectra, and additional theoretical calculations.

[34] V. Dediu, C. Ferdeghini, F. C. Matacotta, P. Nozar, and G. Ruani, Jahn-Teller dynamics in charge-ordered manganites from Raman spectroscopy, Phys. Rev. Lett. **84**, 4489 (2000).

[35] J. Zhang, P. Dai, J. A. Fernandez-Baca, E. W. Plummer, Y. Tomioka, and Y. Tokura, Jahn-Teller phonon anomaly and dynamic phase fluctuations in $La_{0.7}Ca_{0.3}MnO_3$, Phys. Rev. Lett. **86**, 3823 (2001).

[36] H. A. Jahn and E. Teller, Stability of polyatomic molecules in degenerate electronic states - I—Orbital degeneracy, Proc. R. Soc. London, Ser. A **161**, 220 (1937).

[37] D. Gyepesová and V. Langer, $Ca_{10}(Cr^{V}O_4)_6(Cr^{VI}O_4)$, a disordered mixed-valence chromium compound exhibiting inversion twinning, Acta Crystallogr., Sect. C **69**, 111 (2013).

[38] L. Martıń-Carrón and A. de Andrés, Raman phonons and the Jahn-Teller transition in $RMnO_3$ manganites, J. Alloys Compd. **323-324**, 417 (2001).

[39] L. Martín-Carrón and A. de Andrés, Melting of the cooperative Jahn-Teller distortion in $LaMnO_3$ single crystal studied by Raman spectroscopy, Eur. Phys. J. B **22**, 11 (2001).

[40] T. Malcherek, B. Mihailova, and M. D. Welch, Structural phase transitions of clinoatacamite and the dynamic Jahn-Teller effect, Phys. Chem. Miner. **44**, 307 (2017).

[41] G. A. Gehring and K. A. Gehring, Co-operative Jahn-Teller effects, Rep. Prog. Phys. **38**, 1 (1975).

[42] M. D. Kaplan and B. G. Vekhter, *Cooperative Phenomena in Jahn-Teller Crystals* (Plenum, New York, 1995).

[43] R. J. Elliott, R. T. Harley, W. Hayes, and S. R. P. Smith, Raman scattering and theoretical studies of Jahn-Teller induced phase transitions in some rare-earth compounds, Proc. R. Soc. London, Ser. A **328**, 217 (1972).

[44] L. J. P. Ament, M. van Veenendaal, T. P. Devereaux, J. P. Hill, and J. van den Brink, Resonant inelastic x-ray scattering studies of elementary excitations, Rev. Mod. Phys. **83**, 705 (2011).

[45] E. Saitoh, S. Okamoto, K. T. Takahashi, and K. Tobe, Observation of orbital waves as elementary excitations in a solid, Nature (London) **410**, 180 (2001).

[46] J. van den Brink, Orbital excitations in $LaMnO_3$, Phys. Rev. Lett. **87**, 217202 (2001).

[47] Y. Aoki, H. Konno, H. Tachikawa, and M. Inagaki, Characterization of $LaCrO_4$ and $NdCrO_4$ by XRD, Raman spectroscopy, and *ab initio* molecular orbital calculations, Bull. Chem. Soc. Jpn. **73**, 1197 (2000).

[48] Y. Aoki and H. Konno, Synthesis and structure of novel Cr^{V}-Cr^{VI} mixed valence compounds, $Nd_{1-x}Ca_xCrO_4$ ($x =$ 0.02–0.20), J. Solid State Chem. **156**, 370 (2001).

[49] W. J. Brya, Polarized Raman scattering in transparent polycrystalline solids, Phys. Rev. Lett. **26**, 1114 (1971).

[50] P. G. Klemens, Anharmonic decay of optical phonons, Phys. Rev. **148**, 845 (1966).

[51] O. V. Misochko, E. Ya. Sherman, N. Umesaki, K. Sakai, and S. Nakashima, Superconductivity-induced phonon anomalies in high-T_c superconductors: A Raman intensity study, Phys. Rev. B **59**, 11495 (1999).

[52] R. B. Stinchcombe, Ising model in a transverse field: I. Basic theory, J. Phys. C: Solid State Phys. **6**, 2459 (1973).

[53] A. Seth, Fractionalisation in spin-orbit coupled magnetic insulators, Doctoral dissertation, International Centre for Theoretical Sciences, Tata Institute of Fundamental Research, 2022, https://thesis.icts.res.in/sites/default/files/2022-10/Final%20thesis_Arnab%20Seth.pdf.